Title

Cyclable Condensation and Hierarchical Assembly of Metastable Reflectin Proteins, the Drivers of Tunable Biophotonics*

Journal

Journal of Biological Chemistry, 291(8)

ISSN

0021-9258

Authors

Levenson, Robert
Bracken, Colton
Bush, Nicole
et al.

Publication Date

2016-02-01

DOI

10.1074/jbc.m115.686014

Peer reviewed

THE JOURNAL OF BIOLOGICAL CHEMISTRY VOL. 291, NO. 8, pp. 4058–4068, February 19, 2016

Cyclable Condensation and Hierarchical Assembly of Metastable Reflectin Proteins, the Drivers of Tunable Biophotonics*

Received for publication, August 17, 2015, and in revised form, December 5, 2015 Published, JBC Papers in Press, December 30, 2015, DOI 10.1074/jbc.M115.686014

Robert Levenson, Colton Bracken, Nicole Bush, and Daniel E. Morse[1]

From the Department of Molecular, Cellular, and Developmental Biology, University of California, Santa Barbara, California 93106-5100

Reversible changes in the phosphorylation of reflectin proteins have been shown to drive the tunability of color and brightness of light reflected from specialized cells in the skin of squids and related cephalopods. We show here, using dynamic light scattering, electron microscopy, and fluorescence analyses, that reversible titration of the excess positive charges of the reflectins, comparable with that produced by phosphorylation, is sufficient to drive the reversible condensation and hierarchical assembly of these proteins. The results suggest a two-stage process in which charge neutralization first triggers condensation, resulting in the emergence of previously cryptic structures that subsequently mediate reversible, hierarchical assembly. The extent to which cyclability is seen in the *in vitro* formation and disassembly of complexes estimated to contain several thousand reflectin molecules suggests that intrinsic sequence- and structure-determined specificity governs the reversible condensation and assembly of the reflectins and that these processes are therefore sufficient to produce the reversible changes in refractive index, thickness, and spacing of the reflectin-containing subcellular Bragg lamellae to change the brightness and color of reflected light. This molecular mechanism points to the metastability of reflectins as the centrally important design principle governing biophotonic tunability in this system.

Cephalopods (squids, octopi, and cuttlefish) are well known for their diversity of light-manipulating, pigment-based, and nano-structural systems used for camouflage and underwater communication (1, 2). Of these systems, the dynamically tunable structural color of certain squids holds great interest as models for next-generation tunable optical materials and devices (3, 4). Reflectins are a class of proteins originally identified in the reflective tissue of the Hawaiian bobtail squid, *Euprymna scolopes* (5), and have since been found in multiple squid species, including the pelagic Pacific and Atlantic squids *Doryteuthis opalescens* and *Doryteuthis pealeii*, respectively (6–8). In these latter two species, the reflectins constitute the principal constituents of the dynamically controlled subcellular Bragg reflector lamellae responsible for the tunable color and intensity of reflected light in "iridocyte" cells (8) and the subcellular vesicles responsible for switchable bright white Mie scattering in specialized "leucophore" cells in females of the Pacific species (the only example, to our knowledge, of switchable broadband reflectance in molluscs) (6). Reflectins are also found, although in a different molar ratio, in the static (non-tunable) Bragg lamellae of fixed-color iridocytes in this species (7).

Reflectance from both the tunable iridocytes and switchable leucophores is activated by the diffusion of acetylcholine (ACh)[2] (8, 9), recently discovered to be released from fine neuronal processes innervating local areas of the squid skin (10). In the tunable iridocytes, it has been shown that the action of ACh is mediated by a muscarinic ACh receptor (9) that, in turn, activates a G protein-phospholipase-Ca^{2+}-calmodulin-mediated signal transduction cascade. This cascade culminates in the activation of specific protein kinases (and phosphatases) to dramatically change the pattern of phosphorylation of the four different reflectins located in the Bragg lamellae (7, 8, 11). Inhibition of this ACh-activated phosphorylation has been shown to block the ACh-activated changes in iridescence, establishing the requirement for phosphorylation (8). The four reflectins isolated from iridocytes in the non-reflective state have been found to be highly positively charged (computed pI values range from 8.6–8.9), with addition of the negative charges upon phosphorylation essentially neutralizing the proteins (7, 8). We hypothesized that the reflectins are therefore in a state of Coulombic repulsion in the non-reflective state, with phosphorylation overcoming this repulsion, allowing the reflectins to condense and assemble. This explanation is consistent with the electron micrographic images first obtained by Hanlon and coworkers (12), showing that ACh activation of reflectance proceeds with condensation of the intralamellar proteins and subsequent shrinkage of the Bragg lamellae and confirmed by our subsequent microspectrophotometric analyses showing that the refractive index inside the reflectin-containing Bragg lamellae increases progressively, therefore activating and progressively increasing the intensity of reflectance at each of the membrane-bound interfaces with the extralamellar spaces (13, 14).

* This work was supported by grants from the Office of Naval Research via a Multidisciplinary University Research Initiative award to Duke University (N00014-09-1-1053) and the Army Research Office (W911NF-10-1-0139) (to D. E. M.). Use of the University of California, Santa Barbara, Materials Research Laboratory Shared Experimental Facilities, a member of the National Science Foundation-funded Materials Research Facilities Network, was supported by the Materials Research Science and Engineering Center Program of the National Science Foundation under Materials Research Award 1121053. The authors declare that they have no conflicts of interest with the contents of this article.

[1] To whom correspondence should be addressed: d_morse@lifesci.ucsb.edu.

[2] The abbreviations used are: ACh, acetylcholine; DLS, dynamic light scattering.

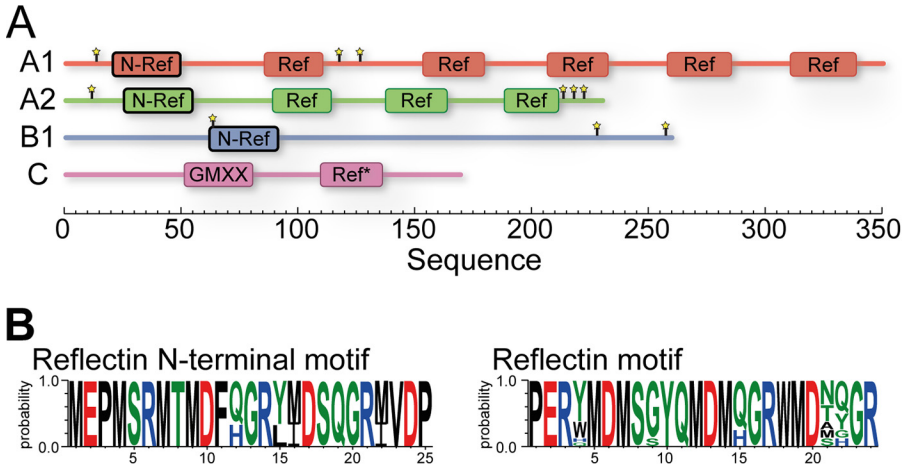

FIGURE 1. *A*, schematic of the four *D. opalescens* reflectin proteins, showing the number and locations of the two types of canonical reflectin motifs, the regular reflectin motifs (*Ref*), and the N-terminal reflectin motifs (*N-Ref*). Previously identified reflectin phosphorylation sites are labeled with *stars* (7, 8). The GM*XX* motif in reflectin C is a unique region of increased overall hydrophobicity composed of a four-amino acid repeat, where *X* represents less conserved locations within the repeat (7). Additionally, the reflectin motif of reflectin C is marked with an *asterisk* to indicate that it contains substantial deviations in sequence not observed in any other reflectin motifs. Sites of phosphorylation in reflectin C have not yet been identified. *B*, sequence logos of the N-terminal and regular reflectin motifs. The logograms were formed from alignment of motifs from *D. opalescens* and the nearly identical *D. pealeii* reflectins (irregular motif in reflectin C excluded) (31).

A corollary of this condensation is the predicted masking of surface charges on the reflectins that would drive an efflux of small counterions across the lamellar membrane to maintain electrostatic neutrality, with this, in turn, driving a Gibbs-Donnan-mediated efflux of water to maintain osmotic equilibrium, therefore accounting for the simultaneous shrinkage of the thickness and spacing of the Bragg lamellae. Confirming these hypotheses, we observed the predicted efflux of water from the ACh-activated iridocytes and its re-entry upon reversal of the ACh effect using D_2O as a tracer (11). Focused ion beam sectioning and transmission electron microscopy imaging revealed that the tunable Bragg lamellae are formed by a series of accordion-like pleats of the cell membrane (11), therefore accounting for the rapid and uniform efflux and reuptake of water and the resulting changes in lamellar dimensions that drive the tunable biophotonics. Our preliminary evidence so far supports a similar molecular mechanism driving the switchable white reflectance from the dynamic leucophores, with the observed difference in the subcellular structures containing the reflectins accounting for the difference in the resulting photophysics. Therefore, upon activation with ACh, the reflectins within the subcellular vesicles are seen to condense and assemble, with resulting Gibbs-Donnan-mediated dehydration causing the vesicles to become pycnotic, thereby increasing the refractive index and changing the vesicle shape to activate broadband Mie scattering (6).

Reflectins constitute a unique family of proteins, enriched in methionine, histidine, lysine, and tyrosine and relatively deficient in other residues, including the large hydrophobics isoleucine, leucine, and valine (5, 8). They also are notable for their content of one or more canonical sequence motifs that are especially enriched in methionine residues. There are two forms of these motifs, one that occurs near the N terminus of the protein and another that is distributed throughout the rest of the protein in variable numbers depending on the type of reflectin. (Fig. 1). The structural or functional role of these motifs is still unknown. *D. opalescens* iridocytes contain four types of reflectin proteins, A1, A2, B, and C, that vary in length, composition, and the number and locations of reflectin motifs. Prior investigations have revealed interesting optical and proton-conducting properties of thin films of these recombinant proteins and their peptide fragments, with consistent observations of low solubility and an absence of any significant secondary structure (15–19). Given their low sequence complexity and lack of large hydrophobic residues necessary for folding, reflectins can be categorized within the increasingly important class of intrinsically disordered proteins.

Although signal-activated phosphorylation is the oldest known and one of the most widely distributed regulatory mechanisms of protein structure and function (20), recent research has focused on the central importance of structural metastability as a key enabler of switchable control in regulated proteins (21–24). Using pH to manipulate the charge on the proteins as a surrogate for the phosphorylation that regulates reflectin structure and function *in vivo*, we show here, with the purified recombinant four reflectins from the tunable iridocytes of *D. opalescens*, that the reversible condensation and hierarchical assembly of these proteins are exquisitely controlled by charge neutralization, confirming the central importance of the metastability of these drivers of tunable, structural biophotonics.

Experimental Procedures

Reflectin Expression and Purification—Codon-optimized reflectin sequences corresponding to the previously determined sequences of *D. opalescens* reflectins A1, A2, B, and C, inserted into a kanamycin-resistant expression plasmid, were obtained from DNA 2.0 Inc. (San Francisco, CA). Although the originally obtained plasmids contained N-terminal His_6 affinity tags with tobacco etch virus protease linkers, these segments were removed by oligonucleotide-directed mutagenesis, and only the native-like constructs were used for all experiments reported here. Protein expression and purification followed methods published previously (16). Plasmids were transformed into Rosetta 2 (DE3) cells and plated onto agarose plates con-

taining 50 mg/ml kanamycin and 37 mg/ml chloramphenicol. Selected colonies were then grown overnight in 3 ml of LB liquid culture with kanamycin and chloramphenicol. The next day, saturated cultures were transferred into 1 liter of LB medium and grown until reaching an A_{600} of ~0.6. Expression was then induced by the addition of 1 mM isopropyl 1-thio-β-D-galactopyranoside (final concentration). After ~6 h of expression, cells were pelleted by centrifugation for 10 min at 5000 × *g*, resuspended in fresh medium to wash cells, and then centrifuged again. Cell pellets containing expressed reflectin inclusion bodies were stored at −80 °C until use.

Purification of reflectins followed a procedure published previously (16). Briefly, cell lysis and inclusion body purification were performed using BugBuster medium (Novagen, Inc., Madison, WI) as recommended by the manufacturer. Purified inclusions bodies were resolubilized at room temperature in 5% acetic acid, 8 M urea, 6 M guanidinium-HCl solution. Guanidinium HCl was then removed by dialysis in 5% acetic acid, 8 M urea before loading solubilized protein on a HiTrap XL cation exchange column. Protein was eluted by a step gradient of increasing guanidinium-HCl concentration (0.3–0.6 M) and then dialyzed once more against 5% acetic acid, 8 M urea or diluted into this buffer and then reconcentrated using a centrifugal concentrator. Protein was then loaded on a MonoS cation exchange column and eluted with a similar step gradient of increasing guanidinium-HCl. On both ion exchange columns, distinct populations of reflectin eluted at different levels of ionic strength. Only the first population that eluted at lowest ionic strength was selected for further use. The eluted reflectin protein was then loaded onto a reverse-phase HPLC column, buffer-exchanged into H_2O/0.1% TFA, and eluted with an increasing gradient of acetonitrile (0–95%) in 0.1% TFA. Collected reflectin fractions were lyophilized and stored at −80 °C until use. Purity was assessed by SDS-PAGE using 10% Tris acetate gels (Life Sciences) run according to the instructions of the manufacturer and stained with Coomassie Brilliant Blue.

Reflectin Solubilization, Buffer Preparation, and Protein Control Solution—Lyophilized reflectins were dissolved in MilliQ water that had been purified by passage through 0.02-μm-pore size filters (Waters Corp., Milford, MA) and then clarified by centrifugation for 15 min or more at 18,000 × *g*. Concentrations were determined using absorption extinction coefficients calculated for each reflectin, which all contained numerous UV-absorptive amino acids. All reflectin stocks were diluted to 81 μM. To create buffer solutions, 250 mM stocks were made at appropriate pH values, as confirmed by measurement with a pH meter. All buffer stocks and water were filtered through 0.02-μm-pore size filters before use. However, because passage of water-solubilized reflectins through 0.02- or 0.22 μm filters resulted in the formation of larger-sized reflectin particles, the proteins were instead clarified by centrifugation for 15 min or more at 18,000 × *g* in a microcentrifuge before use.

We employed an empirically determined minimal concentration of buffer (5 mM MOPS, pK_a 7.28 at 25 °C) that could adequately buffer the protein solutions with only slight perturbations of ionic strength across the range of pH values tested. Unless noted otherwise, the 81 μM individual reflectin stocks were diluted 9-fold into premixed buffer stocks to provide final diluted buffer concentrations of 5 μM and final reflectin concentrations of 9 μM. In the case of experiments using defined mixtures of reflectins, the individual reflectins in water were first combined, which did not result in any observable assembly by dynamic light scattering (data not shown), and then diluted and mixed extensively by pipetting with an appropriate amount of buffer to yield a final buffer concentration of 5 mM. For reversibility tests, 250 mM acetic acid (pH 4.5), was added quickly to the test samples and mixed extensively by pipetting and stirring to yield a final acetate concentration of 15 mM. For all experiments, reflectin stocks and buffers were pre-equilibrated at 25 °C before mixing and analysis. Between experiments, proteins and stocks were stored overnight at 4 °C before re-equilibration at 25 °C prior to use. Both BSA and horse skeletal myoglobin, used as non-aggregating protein controls, were obtained as purified protein (Sigma-Aldrich, St. Louis, MO) and dissolved in water or buffer at a final concentration equal to that of the reflectins unless noted otherwise. For mixtures of reflectins, the four reflectins were combined in ratios corresponding to those observed in specific cell types (7): dorsal A1:A2:B:C molar ratio, 1:0.9:3.1:3.6; ventral molar ratio, 1:3.3:1.4:2.4. These were combined in water before dilution into a buffer of the appropriate pH.

Turbidimetric and Centrifugation Assays—Reflectins were diluted and mixed in buffers of varying pH values as described above to yield total sample volumes of 45 μl. After 5-min incubation periods, portions of each sample were analyzed for turbidity with a spectrophotometer (ThermoScientific NanoDrop, Rochester, NY) by measuring absorbance at 350 nm. The remainder of the sample was centrifuged for 10 min at 18,000 × *g*, and the supernatant was analyzed spectrophotometrically (under UV light) to quantify the remaining reflectin by comparing absorbance at 280 nm with a sample of protein dissolved in water.

Dynamic Light Scattering—Samples were prepared as described above to yield final sample volumes of 45 μl. 40 μl of prepared buffer was loaded in disposable DLS cuvettes, to which 5 μl of reflectin or control protein (or water) was added and mixed rapidly by pipetting and stirring. Buffers, samples, disposable cuvettes, and the DLS spectrometer cuvette holder (Malvern Zetasizer ZS, Worcestershire, UK) were all pre-equilibrated to 25 °C immediately prior to mixing. DLS measurements were initialized approximately 1 min after mixing and conducted at 25 °C. All measurements and volume fittings were performed with Zetasizer software (version 7.11).

For the cyclability test, 90-μl samples of 9 μM reflectin A1 or 9 μM protein with a ratio of reflectin A1, A2, B, and C as found in dorsal iridocytes was prepared initially in 5 mM acetic acid (pH 4.5). Each sample was placed in a Slide-A-Lyzer™ MINI dialysis cup (Life Technologies) and dialyzed overnight into a ≥350-fold excess of 5 mM MOPS (pH 7.5). Samples were retained in their dialysis cups in dialysis buffer until immediately before measurement. To reverse assembly, 250 mM acetic acid (pH 4.5) stock was added to yield a final acetate concentration of 15 mM. Cycles were repeated by dialysis into fresh MOPS at pH 7.5 and reacidified as above. Samples were analyzed by DLS at the start of the experiment and then after each day-long dialysis and immediately after each reacidification.

Transmission Electron Microscopy—Fresh reflectin A1 assemblies were generated as described above. Samples were diluted 2- to 8-fold in 5 mM MOPS buffer of appropriate pH immediately prior to application on glow-discharged 400-mesh carbon film-coated grids (Electron Microscopy Sciences, Hatfield, PA). 5 μl of diluted reflectin was applied and allowed to rest approximately 1 min before removal of excess sample by wicking with filter paper. Samples were stained by touching the grids three times with 20-μl drops of freshly filtered 1.5% uranyl acetate solution and allowing the drops to remain for 15 s each time before removal of excess stain. Images were acquired on a FEI Tecnai G2 Sphera microscope working at 200 kV.

Fluorescence—Fluorescence measurements were performed with samples, buffers, and a spectrophotometer (Varian Cary Eclipse) at 23–24 °C. Water-solubilized reflectin A1 (22 μl) was mixed with 176 μl of buffer to give a final concentration of 9 μM. All measurements were performed with both excitation and emission slits set at a 5-nm width. For experiments with 1-anilino-8-naphthalenesulfonate (ANS), a 10 mM stock of this indicator was prepared freshly, filtered through a 0.22-μm filter, and diluted to 50 μM in either water or 5 mM MOPS (pH 6.5). Reflectin A1 (22 μl) was then added to 176 μl of these diluted ANS solutions.

Results

Reflectin Purification and Characterization of Unassembled States—The *D. opalescens* reflectins A1, A2, B, and C were expressed in *Escherichia coli* from recombinant plasmids with sequences corresponding exactly to those determined for the native proteins with codons optimized for expression in the bacterial host (7). Consistent with previous reports, the recombinant reflectins were recovered as insoluble inclusion bodies, solubilized under strongly denaturing conditions, purified chromatographically, lyophilized, and stored at −80 °C until resolubilization in water, as described under "Experimental Procedures." SDS-PAGE analysis of the purified reflectins is shown in Fig. 2*A*. All four reflectins showed good solubility at the concentration ranges used here. The pH values of these resolubilized reflectins were measured as 4–5.

Dynamic light scattering analyses showed that each of the reflectin preparations was monodisperse, with the radius of hydration (R_H) in water decreasing progressively with concentrations above ~10 μM (data not shown). Accordingly, in view of this likely effect of molecular crowding of the flexible, positively charged protein chains, all experiments began with the reflectins at or below this initial concentration in buffer, as noted.

Turbidimetric Analyses of Charge-dependent Assembly—Turbidimetric analyses (Fig. 2*B*) revealed that each of the reflectins showed progressive aggregation or assembly as a function of increasing pH, with an inflection point near charge neutrality. Centrifugation of these preparations resulted in nearly complete removal of reflectins at higher pH values, confirming the larger particle sizes at higher pH values (Fig. 2*C*). In contrast, neither myoglobin nor BSA, proteins that are predominantly monomeric, showed any changes in these analyses (myoglobin data not shown).

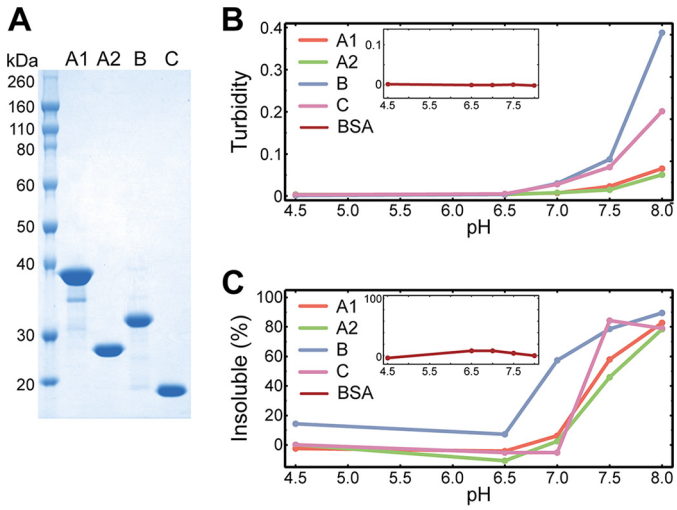

FIGURE 2. *A*, SDS-PAGE of purified reflectin proteins stained with Coomassie Brilliant Blue. *B*, turbidity (optical density at λ = 350 nm) of the indicated reflectins as a function of pH. Each measurement was taken 5 min after dilution of water-dissolved reflectin into buffer at the indicated pH. *C*, insoluble reflectin (samples from *A* pelleted after centrifugation for 10 min), as determined by absorbance at 280 nm. *Insets*, results for the BSA control. Shown are typical results from duplicate experiments.

Dynamic Light Scattering—We used DLS to further characterize the size distribution of particles formed by the reflectins as a function of charge neutralization and its reversal. Fig. 3*A* shows intensity distributions of assembled reflectin A1 at varying pH values. In most samples, signals for two distinct peaks were observed, corresponding to smaller and larger particle assemblies of substantially different sizes. As can be observed, intensity signals between the relevant reflectin assembly and other larger scattering particles can be clearly resolved, allowing for clear determination of R_H. Because the scattering intensity is related exponentially to the size of a spherical particle, volume analysis of the data (Fig. 3*B*) shows these larger assemblies to be minor species (usually <1–5% and occasionally as high as ~15%) of the total protein population. Our assumption of roughly spherical particles, necessary for accurate volume analysis, is justified by electron microscopy visualization of these assemblies (see below). DLS analysis showed the majority reflectin assembly species to be relatively monodisperse, as exemplified by Fig. 3*B* for reflectin A1. The other reflectins exhibited similar distributions, although it is important to note that DLS cannot resolve independent signals from particles in this size range differing in R_H by less than 2-fold. Reflectin assemblies were observed to be stable over time, as shown for reflectin A1 (Fig. 3*C*), although the largest particles formed by reflectins B and C did begin to fall out of the light path with time because samples were held without mixing. A strong, positive, highly reproducible relationship between pH and particle R_H values was observed for all four reflectins, consistent with the turbidity and centrifugation measurements presented above (Fig. 3*C*). The observed values of R_H were bimodal, with reflectins B and C forming larger particles than those of reflectins A1 and A2 across our pH range. In the pH range of 6.5–7.5, reflectins A1 and A2 formed assemblies ranging in R_H value between ~10–20 nm, whereas reflectins B and C formed assemblies of ca. 60–100 nm. In addition to the pH values shown in Fig. 3, we

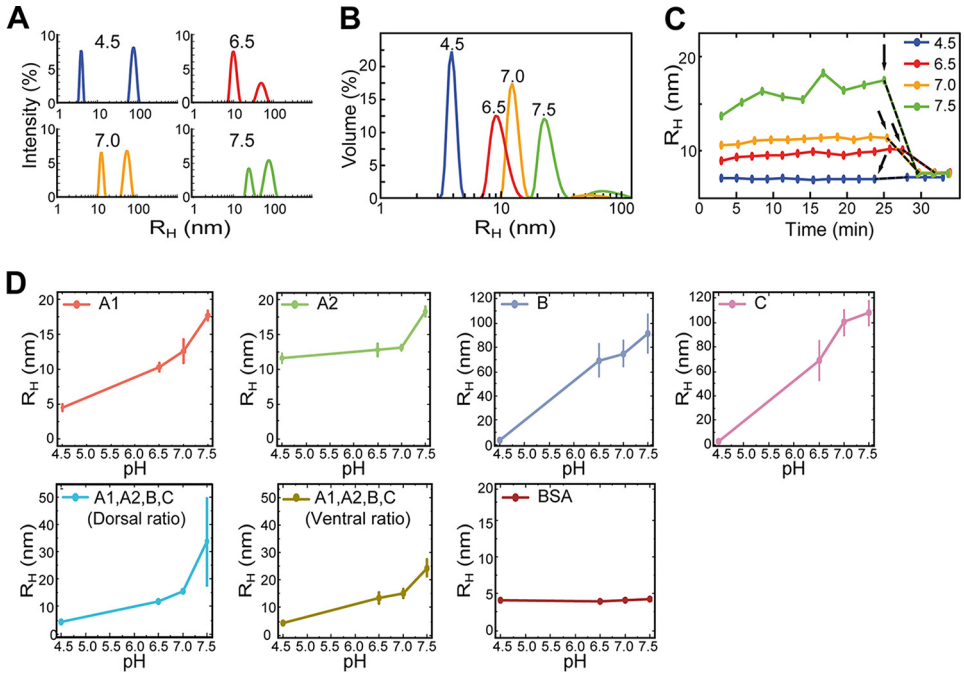

FIGURE 3. **Dynamic light scattering of reflectins as a function of pH.** *A*, intensity distributions of 9 μM reflectin A1 diluted in 5 mM MOPS buffer at the indicated pH values. Representative data from multiple analyses are shown. *B*, DLS volume distributions of same samples as shown in *A*. *C*, time dependence of DLS volumetrically dominant distributions from time of dilution of reflectin A1 into buffer at the indicated pH. Each individual data point is the average of the last 2–3 min of repetitive scattering measurements. *Black arrows* indicate measurements immediately before acidification with 15 mM acetic acid and subsequent equilibration (*black dotted line*) prior to the next DLS measurement. *D*, R_H of individual reflectins or indicated mixtures measured ~20 min after dilution into buffer at the indicated pH. All measurements were replicated at least three times with samples from at least two separate protein purifications and buffer preparations. *Error bars* show mean ± S.D. The individual time courses of particle size for all samples resembled those shown in *C*.

measured R_H values of all reflectins at pH 8.0. However, in contrast to the lower pH values, we encountered significant variance in particle size between experiments for all reflectins at this pH value, although these sizes were always larger than those formed at pH 7.5 (data not shown). We suggest that this increased heterogeneity may be due to the poor buffering ability of 5 mM MOPS at pH 8.0. Compounding this effect, it also is clear that the reflectins become increasingly sensitive to small differences in pH closer to their pIs, as seen in Figs. 2, *B* and *C*, and 3*D*. As expected, the apparent sizes of the assembled complexes of each of the reflectins were found to grow more rapidly and larger when otherwise identical analyses were conducted in progressively increasing ionic strengths of NaCl, KCl, or buffer salts (data not shown). In contrast to the reflectin proteins, BSA showed no substantial changes in R_H, as measured by DLS, across the pH range used in these experiments, whereas myoglobin showed no changes in R_H at pH values of more than 5.5 (myoglobin data not shown).

We also measured the pH-dependent R_H values of mixtures of reflectins corresponding to the molar ratios reported recently from both the ACh-responsive dorsal and ACh-unresponsive ventral iridocytes of the squid (7), analyzed at a total concentration of all four reflectins equal to that of the single reflectins analyzed individually (9 μM) (Fig. 3*C*). Mixtures of the reflectins in molar ratios equal to those observed in both dorsal and ventral iridocytes formed a single signal peak, indicating one distinct population size, as also observed with the individual reflectins. Although the trend of progressive sizes of the resulting assemblies with increasing pH was similar and intermediate to that observed for the individual reflectins, we noted that the largest sizes reached more closely resembled those of reflectins A1 and A2, a point to which we return under "Discussion."

Electron Microscopy—We used transmission electron microscopy to further characterize the reflectin A1 assemblies (Fig. 4). Samples were freshly prepared and examined by DLS before application to grids and negative staining. The assemblies were found to be roughly spherical and relatively monodisperse, with pH-dependent mean diameters in excellent agreement with the DLS measurements. The surface of the A1 assemblies appears to be homogenous, with signs of possible regular substructures discernable at the highest magnification. The monodispersity, spherical shape, and size agreement of these assemblies validates our interpretation of the DLS measurements as discussed above and further confirms the sensitivity of reflectin assembly size to protein net charge.

Reversibility and Cyclability of Reflectin Assembly—Modification of the forgoing DLS analyses was used to monitor the reversibility and cyclability of reflectin assembly in efforts to emulate the cyclability of reflectin condensation and assembly in the tunable squid iridocytes. Addition of acetic acid to return the neutralized and assembled reflectin A1 to a final pH of 4.5 consistently led to disassembly of almost all reflectin particles, resulting in the formation of ~10-nm particles (Figs. 3*C* and 5, *A* and *B*). In contrast, the results of comparable acidification of reflectins A2, B, and C were less consistent, frequently yielding no disassembly (reflectin A2) or partial disassembly (reflectins B and C) (data not shown). Because we suspected that this observed variability was the result of the progressively increased ionic strength of the medium (to which assembly of the

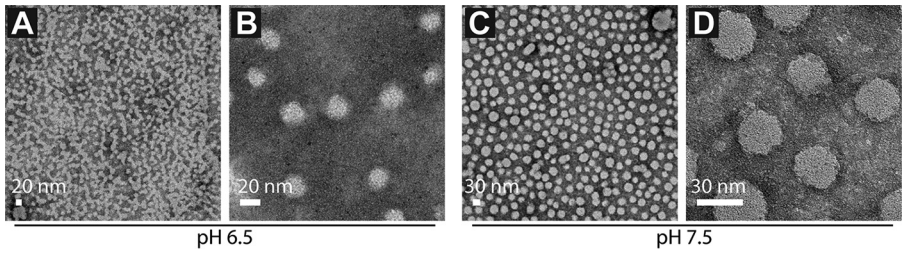

FIGURE 4. **TEMs of reflectin A1 assemblies.** *A* and *B*, reflectin A1 assembled at pH 6.5, imaged at low and high magnification. DLS of the sample prior to grid application showed R_H = 10 nm (diameter = 20 nm). *C* and *D*, reflectin A1 assembled at pH 7.5, imaged at low and high magnification. DLS of the sample prior to grid application showed R_H = 17 nm (diameter = 34 nm).

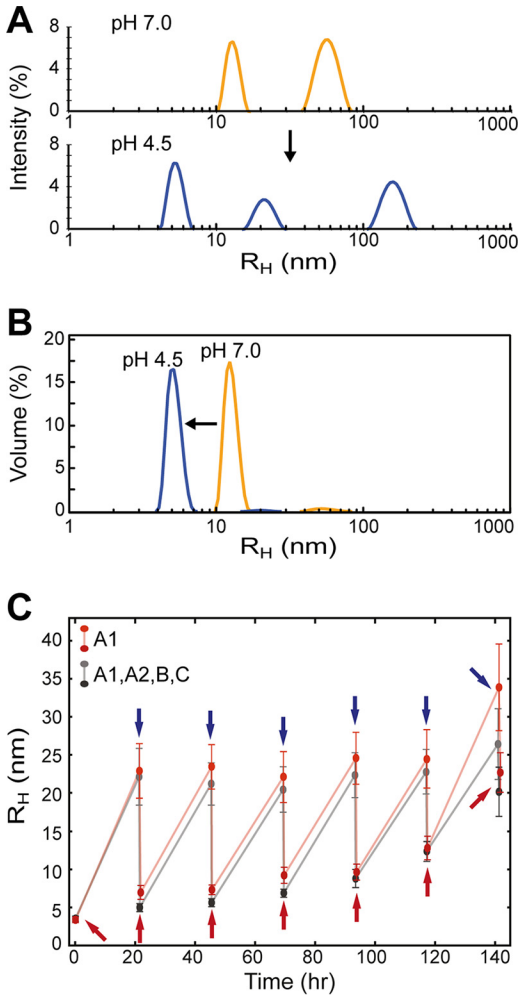

FIGURE 5. **Reflectin assembly, disassembly, and cyclability.** *A*, dynamic light scattering intensity distribution data of assembly and disassembly of 9 μM reflectin A1 first diluted in 5 mM MOPS buffer at pH 7.0 and then immediately after addition of acid to reach 15 mM acetic acid (pH 4.5). The experiments were repeated multiple times. The results shown are representative of A1 at all assembled pH values. pH values are as indicated. *B*, volume distribution of the data in *A*. *C*, cyclability of assembly and disassembly of reflectin A1 and a mixture of the four reflectins in a ratio corresponding to that of the tunable dorsal iridocytes. *Blue arrows* indicate points of measurement of reflectin R_H values followed by addition of a molar excess of acetic acid (pH 4.5). *Red arrows* indicate measurements of reflectin R_H values following partial disassembly. The transition from pH 4.5 to 7.5 was effected by dialysis (see details under "Experimental Procedures"). The R_H shown is for the volumetrically predominant species as determined by DLS. *Error bars* indicate mean ± S.D. of volumetric data within the experiment shown. The results are representative of closely agreeing duplicate analyses.

reflectins is especially sensitive), we replaced this method with one in which cycling between the charged and uncharged states of the proteins was effected by dialysis without increasing ionic strength. Under these conditions, clear evidence for cyclability was seen for both reflectin A1 and for the "physiological mixture" of all four reflectins in a molar ratio equal to that found in the highly tunable and cyclable dorsal iridocytes of *D. opalescens* (Fig. 5*C*) (7). Under these conditions, both the physiological ratio of all four reflectins and reflectin A1 reversibly cycled through multiple cycles of assembly and disassembly, although the extent of dissociation deteriorated progressively with each cycle, with this effect proceeding more rapidly for the mixture than for A1. The sizes of the assembled particles effected by dialysis were slightly smaller than those observed under the assembly conditions used in the previous experiments, possibly because of small differences in pH in the two protocols.

Reflectin A1 Fluorescence—To further probe the nature of the structural changes occurring during assembly, we investigated changes in fluorescence from the tryptophan residues in reflectin A1. Fortuitously, seven of the ten tryptophans in this protein are located within the conserved reflectin motifs, allowing them to serve as useful reporters of changes in the environment of these unique structural domains.

Comparison of the fluorescence spectra shows that, upon assembly of reflectin A1, a moderate ~5-nm blue shift occurs relative to the spectrum of the unassembled protein, indicating a net transfer of the fluorophores to a more hydrophobic environment, as would be expected during protein condensation and assembly (Fig. 6). Significantly, we see that the extent of the blue shift was essentially the same for A1 particles assembled at different pH values. Because the DLS data show that these particles increased progressively in size with increasing pH, this constancy in the observed blue shift indicates that the local environment of the tryptophan probes remained constant even as particles grew bigger. Upon reacidification driving the reflectin to return to the charged state and partial disassembly (as seen in Figs. 3*C* and 5), fluorescence exhibited a small red shift, with the quantum yield slightly higher than in the fully unassembled state observed in water.

We also used the fluorescent probe ANS to investigate changes in reflectin A1 protein structure during assembly (Fig. 7). ANS is a commonly used dye that exhibits a greatly increased fluorescent yield upon binding to exposed hydrophobic protein surfaces (25, 26). As seen in Fig. 7*A*, ANS bound to reflectin A1 in the unassembled state in water, in the partially condensed and assembled state at pH 6.5, and in the acid-dissociated state. ANS emission exhibited both a small blue shift and a large increase in quantum yield when bound to the reflectin in the partially assembled state at pH 6.5 relative to those

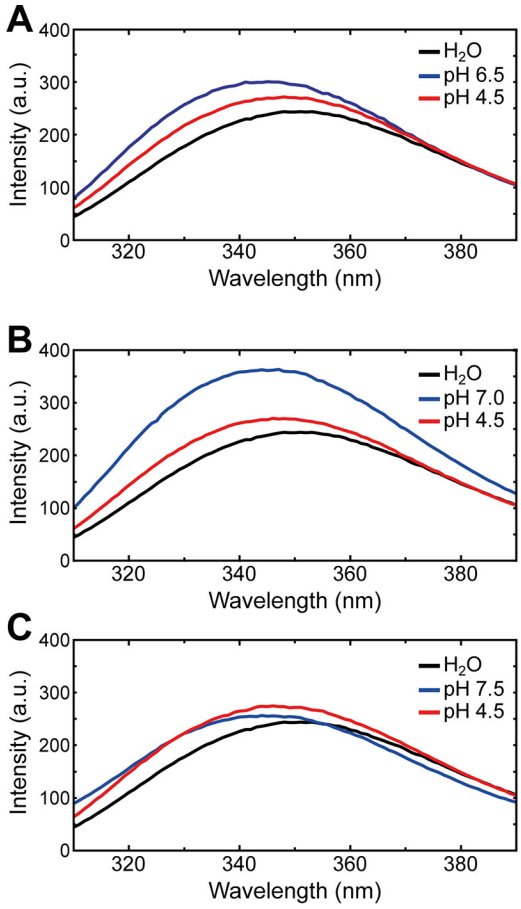

FIGURE 6. **Fluorescence spectra of tryptophan residues in reflectin A1 in the unassembled water-solubilized state, incubated at the indicated pH values, and in the acetic acid-reversed state.** Excitation λ = 295 nm. *A.U.*, arbitrary units.

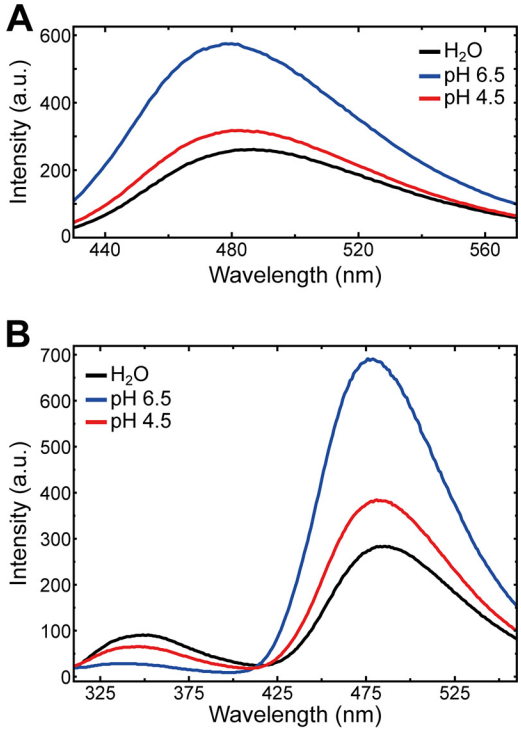

FIGURE 7. *A*, fluorescence of ANS bound to reflectin A1 (excitation λ = 350 nm). ANS was bound to the reflectin in the unassembled water-solubilized state and bound independently to reflectin at pH 6.5, and that sample was then reacidified to pH 4.5 as described under "Experimental Procedures." *B*, fluorescence resonance energy transfer from tryptophan to ANS (excitation at λ = 295 nm). The samples were those described in *A*. *A.U.*, arbitrary units.

features exhibited when bound to the unassembled protein in water, and both of these features were largely reversed when bound to the acid-dissociated protein. These results are similar in form to those exhibited by the native tryptophan fluorescence shown in Fig. 6.

We confirmed the proximity of ANS binding sites and native tryptophans in reflectin A1 through a simple FRET experiment. In the presence of ANS, tryptophan fluorescence was quenched greatly, whereas ANS fluorescence was enhanced at pH 6.5, and this effect was reversed by acidification to pH 4.5 (Fig. 7*B*). These results indicate that the ANS molecules were moved close to one or more tryptophans as charges on the reflectin were neutralized and that this proximity was disrupted when the reflectins were returned to the positively charged state.

Discussion

We investigated the effects of net charge on reflectin assembly through the modulation of external solution pH and provide support for the previous hypothesis, generated from *in vivo* experimentation, that reflectin condensation and subsequent assembly, which govern the dynamic tunability of color and intensity of light reflected or scattered from membrane-enclosed populations of these molecules (6, 11), are driven by charge neutralization. We used this simple method of titration as an *in vitro* surrogate for the signal-activated changes in phosphorylation that drive condensation and assembly of the reflectins *in vivo* (7, 8, 11). Electron microscopy of reflectin A1 assemblies further support the low polydispersity of the discrete particles formed by this method. Although the general biophysical principle analyzed in this work, that proteins aggregate near net neutrality (*i.e.* close to their pI), is a classic one, the reflectins stand out in their exquisitely graduated response and reversibility of condensation and assembly as the net charge diminishes.

Reflectins A1, A2, B, and C showed relatively similar responses to decreases in net charge when analyzed individually, although differences in particle size were seen between the group of reflectins A1 and A2 and the group of reflectins B and C. The latter two reflectins are nearly devoid of non-N-terminal reflectin motifs (*cf.* Fig. 1), with the single motif on reflectin C containing several mutations not observed in the other three proteins. Therefore, it may be possible that the reflectin motifs serve a role in limiting some modes of nonspecific reflectin assembly. This suggestion is supported by our analysis of the mixtures of the four different reflectins tested at two different physiological molar ratios (found in two different classes of iridocytes) in which the presence of reflectins A1 and A2 may have prevented assembly of the larger particles that otherwise would have been formed by reflectins B and C (*cf.* Fig. 3*D*). In support of this suggestion, although transmission electron microscopy images of reflectin B assemblies show that they also form roughly spherical morphologies similar to those observed in reflectin A1 (Fig. 4), the reflectin B assemblies appear to be notably more heterogeneous in diameter, indicating that their assembly may be regulated less tightly because of their content

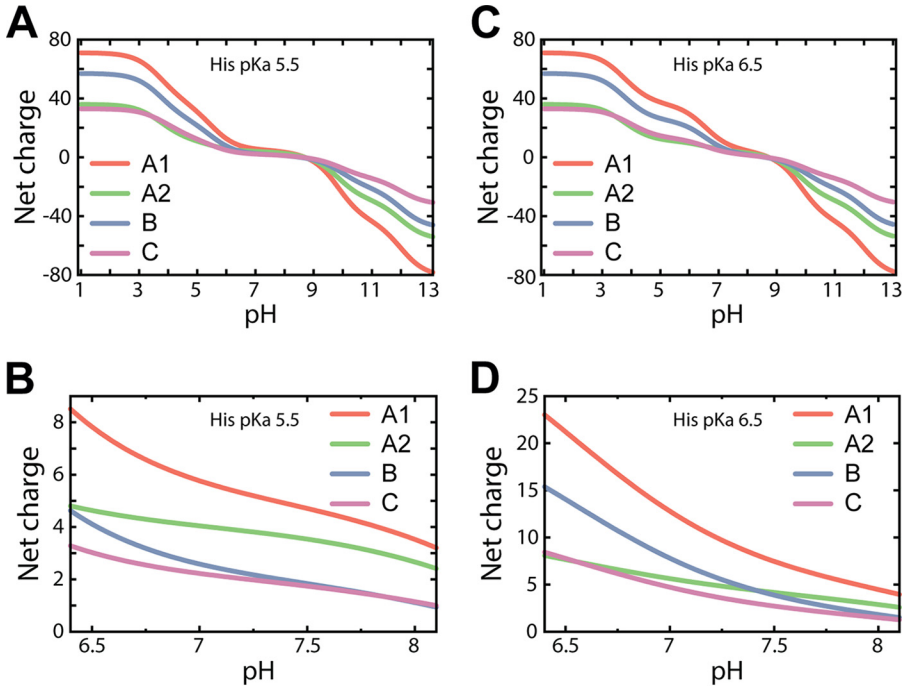

FIGURE 8. *A–D*, calculated reflectin net charge *versus* pH, with assumed histidine pK_as of 5.5 (*A* and *B*) and 6.5 (*C* and *D*). All titratable amino acid pK_as other than histidine are from Ref. 27. The data were calculated by spreadsheet with 0.01-pH unit increments.

of only a single reflectin motif (data not shown). This potential effect of the number of canonical motifs in each of the reflectins is discussed in greater detail below. Essentiality of all four of the reflectins *in vivo* is suggested not only by the significant differences in their sequences and behaviors but also by the discovery that they are distributed differentially within the lumens of the tunable Bragg lamellae, with reflectin C located close to the inner membrane walls of the lamellae and the other reflectins located more uniformly within the lamellar lumen (7). The fact that both mixtures of the four reflectins, in the different molar ratios equal to those found in the tunable dorsal iridocytes and those in the non-tunable ventral iridocytes, responded comparably to pH-induced assembly and disassembly suggests that differences in the ACh receptors, signal transducers, or the charge-regulating enzymes governing reflectin phosphorylation may account for the lesser cholinergic responsiveness of the ventral iridocytes observed *in vivo* (11).

It is clear that the reversible condensation and assembly of the reflectins that we observe driven by titration as a function of pH result from the reversible neutralization of the excess positive charge on the proteins. This conclusion is supported by calculation of the net positive charge on the four reflectins within the pH range probed in these experiments (Fig. 8, *A–D*). Histidine residues, abundantly present in the reflectins (Fig. 9) and with a pK_a of 6.5 in unfolded model peptides, are likely to be the main species undergoing neutralization near this pH (27). Notably, these histidine residues are present almost entirely within the reflectin linker regions, similar to previously identified *in vivo* phosphorylation sites (7, 8). Histidine pK_as are found to have substantial variability in folded proteins, where local environments can cause perturbations by as much as several pH units (28) as a consequence of changes in the activity coefficient of the ionizable proton. In Fig. 8, we show the net charges for the reflectins calculated with the assumption of a uniform histidine pK_a of either 5.5 (*A* and *B*) or 6.5 (*C* and *D*). The divergence we observe between the predicted net charges of reflectins A1/A2 and reflectins B/C at the lower histidine pK_a mimics and may help explain the bimodal distribution of assembly sizes seen by DLS (Fig. 3*D*). This suggests that histidine pK_as may be lowered within the reflectin assemblies or may vary across the polypeptides, enabling a broader relationship between net charge and pH than possible with uniform pK_as. In either case, in correlating the sharp increase in assembly of all reflectins between pH 7 and 8 with the estimated changes in the of number of charges in this range, we see that addition of only one or two phosphates would likely be sufficient to drive structural transition and assembly *in vivo*, in agreement with the small number of site-specific reflectin phosphorylations actually observed (7, 8).

With charge neutralization, the fluorescence of tryptophan residues in reflectin A1 (located primarily in highly conserved sites within the reflectin motifs, see Fig. 9) undergoes a small but significant blue shift that remains constant as pH and particle size increase progressively, indicating that condensation of the protein precedes its hierarchical assembly. The relatively small magnitude of this blue shift indicates that the tryptophan reporters have not been transferred into an entirely hydrophobic environment but are likely to still retain access to the aqueous solvent, possibly through channels of some kind. These results are therefore consistent with the suggestion that the reversible condensation, assembly, decondensation, and disassembly require continued rapid access of kinases and phosphatases to specific phosphorylation sites on the reflectins. Such channels might provide the necessary access (7, 8, 11, 16).

ANS fluorescence indicates that this molecule binds to hydrophobic moieties of reflectin A1 from *D. opalescens* in the

FIGURE 9. **Sequences of the *D. opalescens* reflectins with selected, experimentally identified important residues colored.** Histidine residues are colored *green*, and tryptophan residues are colored *purple*. N-terminal reflectin motifs and regular reflectin motifs are shown highlighted in *bordered* and *unbordered gray*, respectively. In reflectin C, the GM*XX* repeat is highlighted in *brown* (7). Previously identified physiological phosphorylation sites are shown with a *yellow background* (7, 8).

unassembled, partially condensed/assembled, and acid-disassembled states. Significantly, this binding is enhanced even at pH 6.5 (as evident from the changes in quantum yield and blue shift) relative to that at pH 4.5, indicating the neutralization-driven emergence of additional hydrophobic ANS binding sites that precedes significant assembly (compare Figs. 2, 3, and 7). Reflectin A1, like other reflectins, is significantly deficient in large hydrophobic residues (with only one isoleucine, three leucines, and four valines in this 350-residue protein) (7), with other likely binding sites for ANS including the tryptophan and tyrosine residues and/or the methionine-enriched reflectin motifs. Consistent with this suggestion, we see very strong quenching of tryptophan fluorescence in the presence of ANS, indicating that the ANS is bound close to tryptophan. We note that seven of the ten tryptophan residues in the *D. opalescens* reflectin A1 are found within the canonical reflectin repeats (Fig. 9).

Although neural network-based secondary structure prediction algorithms do not predict any organized secondary structure for these reflectin motifs, previous investigations from our laboratory have shown that salt-initiated condensation of reflectin A1 drives the emergence of secondary structure exhibiting the x-ray diffraction signature of β-pleated sheets (16), and our preliminary investigations by CD spectroscopy also support this identification (data not shown). Therefore, it appears to be significant that modeling of the hydrophobic moments of the reflectin sequences suggests that the canonical motifs and other regions have an enhanced capacity to form either amphipathic β sheets or helices (Fig. 10*A*) (28). Extending this finding, simple helical modeling shows how the canonical motifs could possibly form amphipathic helices with moderate hydrophobic moments, as illustrated in Fig. 10*B* (29). It is possible that ANS could bind to the hydrophobic surfaces of such weakly structured, amphiphilic β sheets or helices. The functional advantage of such structures is evident. If neutralization-driven condensation of the reflectins were to drive the reversible emergence of such structures, their phase-segregated (amphiphilic) hydrophobic domains could serve as a kind of "molecular Velcro™," leading to reversible, hierarchical assembly.

Although no signature of helices was found in the wide-angle x-ray scattering analyses that did find β sheet structure in condensed reflectin A1 (16), such helices might form ephemerally as intermediates that are replaced by the final β structures. Quantitative modeling of the energetics of such α helical to β sheet transitions support the feasibility of this suggestion (30). Assuming that synthesis of the reflectins in the endoplasmic reticulum occurs at a pH near 7, then the initial stages of condensation and folding we described are likely to have occurred by the time the reflectins enter the Bragg lamellae. This may explain the punctate "beads on a string" appearance of the pre-activation reflectins observed in electron micrographs of the lamellae (8, 16). The ACh-activated, phosphorylation-mediated neutralization of the reflectins in the physiological range of pH within the lamellae that drive the photonic tuning *in vivo* would therefore be most likely to activate the final stages of condensation and assembly.

Considering this postulated role of the canonical reflectin motifs in mediating assembly, we suggest that the balance between intra- and intermolecular association would govern the size of the assembled complexes of the individual, pure reflectins. Consistent with this suggestion, we note that reflectins B and C, each containing only one canonical motif (Fig. 1*A*), are driven by charge neutralization to assemble to significantly larger sizes than reflectins A1 and A2 (which contain six and four canonical motifs, respectively) (Fig. 3*D*). It is therefore interesting to note that a mixture of the four reflectins in the molar ratio corresponding to that found in the dynamically tunable Bragg lamellae reversibly and cyclably assemble to a size comparable with that of reflectin A1 alone (Figs. 3*D* and 5*C*) and that even a small proportion of reflectin A1 brings the assembly of reflectins B and C under similar size control (data

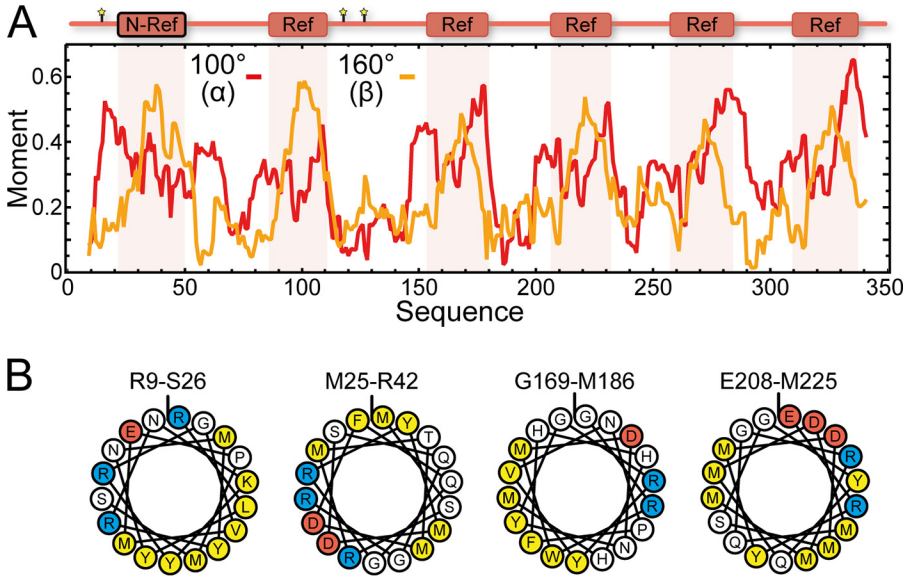

FIGURE 10. *A*, calculation of net hydrophobic moments within reflectin A1 for two sets of residue angles corresponding to the maximal values observed for α helices (100°) and β sheets (160°) (28). Net moments are shown for 18-residue windows centered at those residues. Calculations were performed using EMBOSS (32). *B*, helical projections for selected regions of reflectin A1. *Yellow*, hydrophobic residues; *blue*, positively charged; *red*, negatively charged. A *vertical line* designates the N-terminal residue of the modeled helix. Helical projection images were adapted from the HELIQUEST web server (33).

not shown). The nature of these interactions is the subject of a future communication.

The cyclability we observe shows evidence of progressively deteriorating reversibility, particularly of disassembly (Fig. 5*B*), suggesting that some additional factors or conditions present in the reflectin-mediated system *in vivo* are probably lacking from our partially reconstituted system *in vitro*. In this regard, it is interesting to note the unique distribution of reflectin C, located preferentially at or near the inner faces of the Bragg lamellar membrane (7). This apparent anchoring of one of the constituents of the cyclable assembly might limit nonspecific modes of assembly. Furthermore, the physiological processes governing the charge state of the reflectins by activation of kinases and phosphatases could introduce kinetic and site-specific sequences of events absent from our surrogate *in vitro* global control by pH. Nevertheless, the extent to which cyclability is seen in the *in vitro* formation and disassembly of complexes estimated (from the data in Fig. 5*C*) to contain several thousand reflectin molecules strongly suggests some degree of intrinsic, sequence- and structure-determined specificity of the stages, sites, and processes governing the reversible condensation and assembly of the reflectins.

Recent studies have focused on metastability as a central design principle enabling protein-based systems with reversible and tunable properties. Chilkoti and co-workers (21, 22), working with elastin-like polypeptides, have successfully identified and modeled the amino acid sequences responsible for highly reversible temperature-induced aggregation and disaggregation, with possible medical applications. Additionally, Kaplan and co-workers (23, 24) have shown recently that genetically engineered silk-elastin hybrid proteins can exhibit varied dynamically tunable structures, tensile strengths, and adhesive properties. We suggest that the reflectin proteins that drive tunable biophotonic systems in specialized skin cells of squids exhibit a structural metastability that enables a reversible, tunable/switchable, two-state transition in which charge neutralization first triggers condensation, resulting in the emergence of previously cryptic structures that subsequently mediate reversible, hierarchical assembly. The system we describe here offers a tractable model for further analyses of tunable biophotonics and other tunable biomolecular systems.

Author Contributions—R. L. and D. E. M. designed the experiments and wrote the paper. R. L., C. B., and N. B. performed the experiments. All authors reviewed the results and approved the final version of the manuscript.

Acknowledgments—We thank Dr. D. Mozhdehi (Duke University) and Mary Baum (University of California, Santa Barbara) for review of our manuscript.

Note Added in Proof—While this article was in press we learned of related studies by Naughton *et al.* (K. L. Naughton, L. Phan, Y. Dyke, E. Leung, Q. Lin, C. Zhu, A. Arvai, S. Li, M. E. Pique, M. Naeim, J. P. Kerr, M. J. Aquino, V. A. Roberts, E. D. Getzoff, and A. A. Gorodetsky, X-ray scattering characterization of the cephalopod structural protein Reflectin, submitted for publication) that are consistent with the results published here.

References

1. Hanlon, R. T., Chiao, C.-C., Mäthger, L. M., Barbosa, A., Buresch, K. C., and Chubb, C. (2009) Cephalopod dynamic camouflage: bridging the continuum between background matching and disruptive coloration. *Philos. Trans. R. Soc. Lond. B Biol. Sci.* **364,** 429–437
2. Boal, J. G., Shashar, N., Grable, M. M., Vaughan, K. H., Loew, E. R., and Hanlon, R. T. (2004) Behavioral evidence for intraspecific signaling with achromatic and polarized light by cuttlefish (Mollusca: Cephalopoda). *Behavior* **141,** 837–861
3. Fudouzi, H. (2011) Tunable structural color in organisms and photonic materials for design of bioinspired materials. *Sci. Technol. Adv. Mater.* **12,** 064704
4. Yu, C., Li, Y., Zhang, X., Huang, X., Malyarchuk, V., Wang, S., Shi, Y., Gao,

L., Su, Y., Zhang, Y., Xu, H., Hanlon, R. T., Huang, Y., and Rogers, J. A. (2014) Adaptive optoelectronic camouflage systems with designs inspired by cephalopod skins. *Proc. Natl. Acad. Sci.* **111,** 12998–13003
5. Crookes, W. J., Ding, L.-L., Huang, Q. L., Kimbell, J. R., Horwitz, J., and McFall-Ngai, M. J. (2004) Reflectins: the unusual proteins of squid reflective tissues. *Science* **303,** 235–238
6. DeMartini, D. G., Ghoshal, A., Pandolfi, E., Weaver, A. T., Baum, M., and Morse, D. E. (2013) Dynamic biophotonics: female squid exhibit sexually dimorphic tunable leucophores and iridocytes. *J. Exp. Biol.* **216,** 3733–3741
7. DeMartini, D. G., Izumi, M., Weaver, A. T., Pandolfi, E., and Morse, D. E. (2015) Structures, organization, and function of reflectin proteins in dynamically tunable reflective cells. *J. Biol. Chem.* **290,** 15238–15249
8. Izumi, M., Sweeney, A. M., Demartini, D., Weaver, J. C., Powers, M. L., Tao, A., Silvas, T. V., Kramer, R. M., Crookes-Goodson, W. J., Mäthger, L. M., Naik, R. R., Hanlon, R. T., and Morse, D. E. (2010) Changes in reflectin protein phosphorylation are associated with dynamic iridescence in squid. *J. R. Soc. Interface* **7,** 549–560
9. Mäthger, L. M., Collins, T. F., and Lima, P. A. (2004) The role of muscarinic receptors and intracellular Ca^{2+} in the spectral reflectivity changes of squid iridophores. *J. Exp. Biol.* **207,** 1759–1769
10. Wardill, T. J., Gonzalez-Bellido, P. T., Crook, R. J., and Hanlon, R. T. (2012) Neural control of tuneable skin iridescence in squid. *Proc. R. Soc. B Biol. Sci.* **279,** 4243–4252
11. DeMartini, D. G., Krogstad, D. V., and Morse, D. E. (2013) Membrane invaginations facilitate reversible water flux driving tunable iridescence in a dynamic biophotonic system. *Proc. Natl. Acad. Sci.* **110,** 2552–2556
12. Cooper, K. M., Hanlon, R. T., and Budelmann, B. U. (1990) Physiological color change in squid iridophores: II: ultrastructural mechanisms in *Lolliguncula brevis*. *Cell Tissue Res.* **259,** 15–24
13. Ghoshal, A., Demartini, D. G., Eck, E., and Morse, D. E. (2013) Optical parameters of the tunable Bragg reflectors in squid. *J. R. Soc. Interface* **10,** 20130386
14. Ghoshal, A., DeMartini, D. G., Eck, E., and Morse, D. E. (2014) Experimental determination of refractive index of condensed reflectin in squid iridocytes. *J. R. Soc. Interface* **11,** 20140106
15. Kramer, R. M., Crookes-Goodson, W. J., and Naik, R. R. (2007) The self-organizing properties of squid reflectin protein. *Nat. Mater.* **6,** 533–538
16. Tao, A. R., DeMartini, D. G., Izumi, M., Sweeney, A. M., Holt, A. L., and Morse, D. E. (2010) The role of protein assembly in dynamically tunable bio-optical tissues. *Biomaterials* **31,** 793–801
17. Qin, G., Dennis, P. B., Zhang, Y., Hu, X., Bressner, J. E., Sun, Z., Crookes-Goodson, W. J., Naik, R. R., Omenetto, F. G., and Kaplan, D. L. (2013) Recombinant reflectin-based optical materials. *J. Polym. Sci. B Polym. Phys.* **51,** 254–264
18. Phan, L., Walkup, W. G., 4th, Ordinario, D. D., Karshalev, E., Jocson, J.-M., Burke, A. M., and Gorodetsky, A. A. (2013) Reconfigurable infrared camouflage coatings from a cephalopod protein. *Adv. Mater.* **25,** 5621–5625
19. Ordinario, D. D., Phan, L., Walkup, W. G., 4th, Jocson, J.-M., Karshalev, E., Hüsken, N., and Gorodetsky, A. A. (2014) Bulk protonic conductivity in a cephalopod structural protein. *Nat. Chem.* **6,** 596–602
20. Ubersax, J. A., and Ferrell, J. E., Jr. (2007) Mechanisms of specificity in protein phosphorylation. *Nat. Rev. Mol. Cell Biol.* **8,** 530–541
21. McDaniel, J. R., Radford, D. C., and Chilkoti, A. (2013) A unified model for *de novo* design of elastin-like polypeptides with tunable inverse transition temperatures. *Biomacromolecules* **14,** 2866–2872
22. MacEwan, S. R., and Chilkoti, A. (2014) Applications of elastin-like polypeptides in drug delivery. *J. Control. Release* **190,** 314–330
23. Xia, X.-X., Xu, Q., Hu, X., Qin, G., and Kaplan, D. L. (2011) Tunable self-assembly of genetically engineered silk-elastin-like protein polymers. *Biomacromolecules* **12,** 3844–3850
24. Wang, Q., Xia, X., Huang, W., Lin, Y., Xu, Q., and Kaplan, D. L. (2014) High throughput screening of dynamic silk-elastin-like protein biomaterials. *Adv. Funct. Mater.* **24,** 4303–4310
25. Kundu, B., and Guptasarma, P. (2002) Use of a hydrophobic dye to indirectly probe the structural organization and conformational plasticity of molecules in amorphous aggregates of carbonic anhydrase. *Biochem. Biophys. Res. Commun.* **293,** 572–577
26. Hawe, A., Sutter, M., and Jiskoot, W. (2008) Extrinsic fluorescent dyes as tools for protein characterization. *Pharm. Res.* **25,** 1487–1499
27. Thurlkill, R. L., Grimsley, G. R., Scholtz, J. M., and Pace, C. N. (2006) pK values of the ionizable groups of proteins. *Protein Sci.* **15,** 1214–1218
28. Eisenberg, D., Weiss, R. M., and Terwilliger, T. C. (1984) The hydrophobic moment detects periodicity in protein hydrophobicity. *Proc. Natl. Acad. Sci. U.S.A.* **81,** 140–144
29. Eisenberg, D., Weiss, R. M., and Terwilliger, T. C. (1982) The helical hydrophobic moment: a measure of the amphiphilicity of a helix. *Nature* **299,** 371–374
30. Qin, Z., and Buehler, M. J. (2010) Molecular dynamics simulation of the α-helix to β-sheet transition in coiled protein filaments: evidence for a critical filament length scale. *Phys. Rev. Lett.* **104,** 198304
31. Crooks, G. E., Hon, G., Chandonia, J.-M., and Brenner, S. E. (2004) WebLogo: a sequence logo generator. *Genome Res.* **14,** 1188–1190
32. Rice, P., Longden, I., and Bleasby, A. (2000) EMBOSS: The European Molecular Biology Open Software Suite. *Trends Genet.* **16,** 276–277
33. Gautier, R., Douguet, D., Antonny, B., and Drin, G. (2008) HELIQUEST: a web server to screen sequences with specific α-helical properties. *Bioinformatics* **24,** 2101–2102